Letters

Oscillation Frequency Manipulation in Autonomous WPT Systems With Series–Series Compensation

Yingjun Fei, *Graduate Student Member, IEEE*, Fengwei Chen, Ruozhong Gao, *Student Member, IEEE*, Shijun Zhao, *Graduate Student Member, IEEE*, Chunsen Tang, *Member, IEEE*, and Lei Zhao, *Member, IEEE*

***Abstract*—The autonomous wireless power transfer (WPT) system with series–series compensation has the advantage of the output power being approximately independent of variations in the coupling coefficient and load within the bifurcation region. However, the system encounters the issue of nonuniqueness in steady-state oscillation frequency, influenced by factors, such as varying system parameters, unpredictable external disturbances, and initial conditions. To overcome this issue, this letter proposes a relay-switching technique for manipulating the oscillation frequencies of autonomous WPT systems. This technique utilizes an adjustable relay threshold to dynamically modify the phase relationship between the input voltage and current, guiding the system to operate at the desired oscillation frequency. Complementary to the relay-switching technique, a gain-shaping strategy is presented to enhance the current gain at the target frequency, thereby increasing the possibility of convergence to that frequency. Finally, an experimental setup is built to verify the effectiveness of the proposed method. A video demonstrating the switching of different steady-state oscillation frequencies is attached to this letter.**

***Index Terms*—Autonomous wireless power transfer (WPT) system, gain-shaping, oscillation frequency, relay-switching.**

I. Introduction

AUTONOMOUS wireless power transfer (WPT) systems [1] have received a lot of attention recently, especially with the proposal of parity-time (PT) symmetric systems and the discovery of their excellent properties of output voltage approximately independent of the coupling coefficient and load [2], [3], [4]. An autonomous WPT system can refer to a WPT system that relies on state variables (such as inductance current and capacitance voltage) and its own internal laws to independently maintain stable operation without external interference. The PT symmetric WPT system can be implemented at the circuit level by constructing an autonomous system in which the input voltage is in phase with the current. However, autonomous WPT systems often exhibit bifurcation phenomena and have multiple steady-state oscillation frequencies in the bifurcation region, making it difficult to predict and manipulate the operating state of the system.

In [5], the authors used the stroboscopic mapping method to establish a dynamic model of an autonomous WPT system, and reveal that the autonomous LCL-S WPT system has four steady-state operating points. However, the method for switching between steady-state points is not provided. The introduction of the concept of PT symmetry into the WPT system comprehensively reveals the excellent steady-state characteristics of autonomous systems from the perspective of quantum mechanics [2], but this may be insufficient to characterize the dynamic behavior of the system. In [6] and [7], an autonomous pulse frequency modulation scheme is proposed for output power regulation of the autonomous WPT system, but insightful investigation into the bifurcation and multistable solution phenomena is still missing. In short, there is still a lack of corresponding means to achieve free switching between steady-state solutions.

To fill this gap, this letter proposes an autonomous WPT system with two techniques, i.e., relay-switching and gain-shaping, for oscillation frequency manipulation. The relay-switching technique is the process of adjusting the threshold to change the phase angle between the input current and input voltage, guiding the system to switch among different frequencies at will. The gain-shaping technique is employed to enhance the possibility of system convergence at the target frequency. For example, when the system is desired to work in the inductive region of the low-frequency range, we can reshape the current gain curve so that the current gain near the low-frequency band is greater than that in the high-frequency band, thereby achieving simultaneous operation of the system in a low-frequency and weak inductive state.

II. Proposed WPT System With Relay Switch

An autonomous WPT system with series–series (SS) compensation exhibits typical bifurcation behavior known as forked bifurcation. Within this bifurcation region, there are two steady-state oscillation frequencies [4]. The following discussion will

Manuscript received 24 August 2023; revised 22 September 2023; accepted 5 October 2023. Date of publication 9 October 2023; date of current version 6 December 2023. This work was supported by the National Natural Science Foundation of China under Grants 62073246 and 52277002. *(Corresponding author: Fengwei Chen.)*

The authors are with the School of Automation, Chongqing University, Chongqing 400044, China (e-mail: feiyingjun@cqu.edu.cn; fengwei.chen@cqu.edu.cn; Gaoruozhong@cqu.edu.cn; zsjwpt@cqu.edu.cn; cstang@cqu.edu.cn; lzha915@cqu.edu.cn).

This article has supplementary material provided by the authors and color versions of one or more figures available at https://doi.org/10.1109/TPEL.2023.3323100.

Digital Object Identifier 10.1109/TPEL.2023.3323100

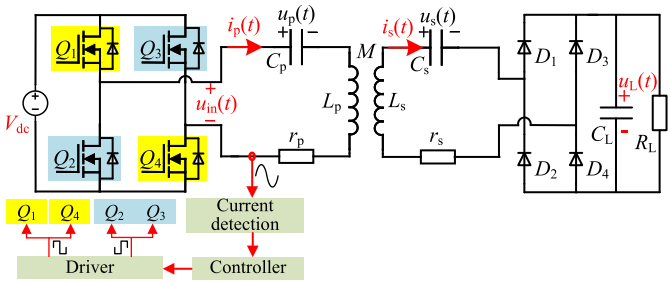

Fig. 1. Circuit diagram of an autonomous WPT system with SS compensation.

provide a detailed introduction to the relay-switching strategy for the SS topology, followed by an explanation of how to utilize this strategy to switch between the two steady-state solutions.

Fig. 1 shows the circuit diagram of an autonomous WPT system with SS compensation. L_p and L_s represent the self-inductances of the primary and secondary coils, respectively. M represents mutual inductance. r_p and r_s represent the equivalent series resistances of the coupled coils. C_p and C_s represent compensation capacitors. R_L represents the load resistance. V_dc represents the dc power source. Q_1–Q_4 represent the switches of the full bridge inverter. D_1–D_4 represent the diodes of the full bridge rectifier. $i_\mathrm{p}(t)$ and $i_\mathrm{s}(t)$ represent the current flowing through the primary and secondary coils, respectively. $u_\mathrm{p}(t)$ and $u_\mathrm{s}(t)$ represent the voltage of the compensating capacitors. $u_\mathrm{L}(t)$ represents the voltage of the filtering capacitor. This WPT system works autonomously where the drive signal of the inverter is generated based on the detection of i_p.

We propose a relay-switching technique for generating the input voltage u_in, instead of the conventional zero-crossing detection. The relay-switching strategy is described in Fig. 2(a), in which u_in is determined by the current state i_p, with the switching times of the MOSFETs determined by $\alpha \cdot i_\mathrm{pm}$ and $-\alpha \cdot i_\mathrm{pm}$. Fig. 2(b) and (c), respectively, illustrates the waveform relationships of input voltage and current for $\alpha > 0$ and $a < 0$. It can be seen that adjusting the threshold α can change the phase between the input voltage and current. The mathematical expression for u_in is presented in (1), where $\cap$ represents the intersection, and $\cup$ represents the union. Here, $\alpha \in [-1, 1]$ represents the threshold of the relay and i_pm represents the peak value of i_p. Note that there is a half-cycle delay in computing i_pm because it requires the values of i_p in the previous half cycle. Under the premise of first harmonic approximation, when $\alpha > 0$, the system operates in the capacitive zone, when $\alpha < 0$, the system operates in the inductive zone, and when $\alpha = 0$, the system operates in the zero-phase-angle (ZPA) state.

Next, the amplitude frequency characteristics of the system will be used to explain how this method achieves switching between stable points. By approximating the variables in the

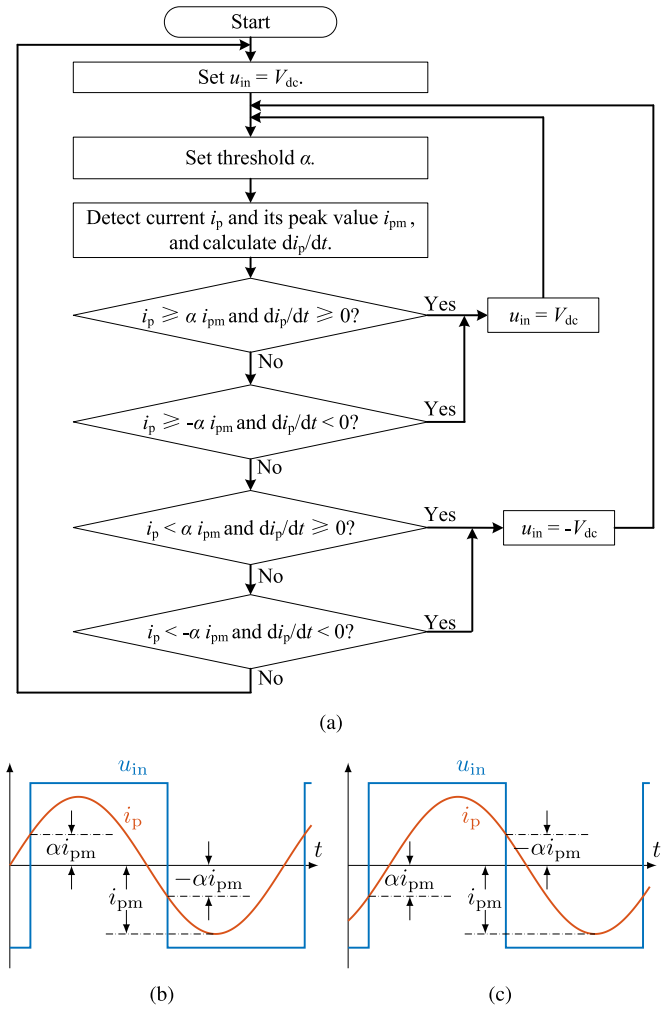

Fig. 2. Relay-switching strategy flowchart and the relationship of input voltage and current under this strategy. (a) Relay-switching strategy flowchart. (b) Relationship between input voltage and current for $\alpha > 0$. (c) Relationship between input voltage and current for $\alpha < 0$.

circuit by their first harmonics, the system input impedance obtained through ac impedance analysis is

$$Z_\mathrm{in} = r_\mathrm{p} + \frac{\omega^2 M^2 (r_\mathrm{s} + R_\mathrm{eq})}{(r_\mathrm{s} + R_\mathrm{eq})^2 + \left(\omega L_\mathrm{s} - \frac{1}{\omega C_\mathrm{s}}\right)^2} + j\left(\omega L_\mathrm{s} - \frac{1}{\omega C_\mathrm{s}} - \frac{\omega^2 M^2 \left(\omega L_\mathrm{s} - \frac{1}{\omega C_\mathrm{s}}\right)}{(r_\mathrm{s} + R_\mathrm{eq})^2 + \left(\omega L_\mathrm{s} - \frac{1}{\omega C_\mathrm{s}}\right)^2}\right) \tag{2}$$

where $R_\mathrm{eq} = 8R_\mathrm{L}/\pi^2$.

$$u_\mathrm{in}(t) = \begin{cases} V_\mathrm{dc} & \{i_\mathrm{p} \geq \alpha\, i_\mathrm{pm} \cap \mathrm{d}i_\mathrm{p}/\mathrm{d}t \geq 0\} \cup \{i_\mathrm{p} \geq -\alpha\, i_\mathrm{pm} \cap \mathrm{d}i_\mathrm{p}/\mathrm{d}t < 0\} \\ -V_\mathrm{dc} & \{i_\mathrm{p} < \alpha\, i_\mathrm{pm} \cap \mathrm{d}i_\mathrm{p}/\mathrm{d}t \geq 0\} \cup \{i_\mathrm{p} < -\alpha\, i_\mathrm{pm} \cap \mathrm{d}i_\mathrm{p}/\mathrm{d}t < 0\} \end{cases} \tag{1}$$

TABLE I
SYSTEM PARAMETERS

L_p, L_s	M	r_p, r_s	C_L	C_p
80.5 μH	30.4 μH	0.1 Ω	300 μF	31.9 nF
R_L	V_dc	f_0	C_s	/
5 Ω	12 V	99.3 kHz	31.9 nF, 28.9 nF	/

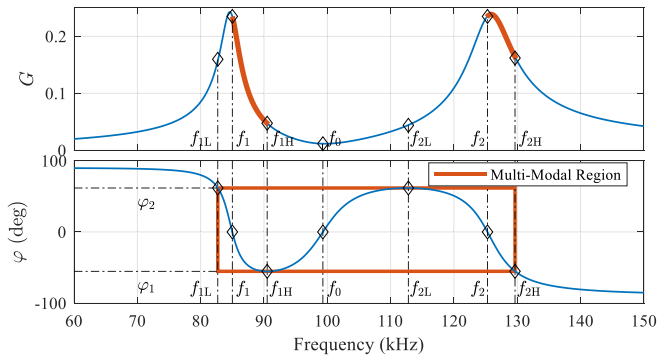

Fig. 3. Amplitude and frequency responses of the system. Top: Input current to voltage amplitude ratio. Bottom: Phase difference between the input current and voltage.

For clarity of exposition, let us denote the gain and phase of Z_in^{-1} as

$$\begin{cases} G(\omega) = \left|Z_\mathrm{in}^{-1}\right| \\ \varphi(\omega) = \angle\left(Z_\mathrm{in}^{-1}\right). \end{cases} \tag{3}$$

The relationship between threshold α in Fig. 2 and phase angle φ is

$$\varphi = \arcsin(\alpha). \tag{4}$$

The parameters listed in Table I are brought into (2) and (3) to compute the frequency response of the system and $C_\mathrm{p} = 1/(\omega_0^2 L_\mathrm{p})$, $C_\mathrm{s} = 1/(\omega_0^2 L_\mathrm{s})$, as shown in Fig. 3. The relationship between the frequencies and phase angles marked in the Fig. 3 is

$$\begin{cases} \dfrac{\partial}{\partial f}\varphi(2\pi f) = 0,\ f = f_{1\mathrm{H}}, f_{2\mathrm{L}} \\ \varphi(2\pi f) = 0,\ f = f_0,\ f_1,\ f_2 \\ \varphi_1 = \varphi(2\pi f_{1\mathrm{H}}),\ \varphi_2 = \varphi(2\pi f_{2\mathrm{L}}). \end{cases} \tag{5}$$

When $\varphi \in [\varphi_1, \varphi_2]$ and $f \in [f_{1\mathrm{L}}, f_{2\mathrm{H}}]$, the system operates in a multimodal region, where there may be multiple steady-state solutions having the same input impedance angle and it is hard to say which solution the system will converge to. At the ZPA frequencies $f_0 = 99.3$ kHz, $f_1 = 84.99$ kHz, and $f_2 = 125.30$ kHz, we have $G(f_1) \approx G(f_2) \gg G(f_0)$, and f_1 and f_2 are stable solutions, while f_0 is an unstable solution [4]. That is to say, when the autonomous system is desired to operate in ZPA state, the oscillation frequency can either be f_1 or f_2. The switching between two frequencies is achieved by adjusting the control variable α to transition the working state of the system from a single-modal region to a multimodal region. If the system is expected to operate on f_1, the initial value of α can be taken as a value greater than $\sin(\varphi_2)$ and gradually decrease to 0. Conversely, if the system is expected to operate on f_2, the initial value of α can be taken as a value less than $\sin(\varphi_1)$ and then gradually increase to 0.

III. Oscillation Frequency Manipulation

In this section, two methods for oscillation frequency manipulation will be presented: one is the aforementioned threshold control method, and its rationale will be explained in more details in the first section, while the other is the more powerful gain shaping method that is to be presented in the second section.

A. Oscillation Frequency Manipulation Via Threshold Control

The autonomous system shown in Fig. 1 and the control strategy shown in Fig. 2 can be considered as a piecewise linear switching system, which has four modes as follows: Mode 1: Q_1, Q_4 ON and D_1, D_4 ON; Mode 2: Q_1, Q_4 ON and D_2, D_3 ON; Mode 3: Q_2, Q_3 ON and D_2, D_3 ON; Mode 4: Q_2, Q_3 ON and D_1, D_4 ON. The switching of the modes depends on the state i_p and i_s. The complexity of the system lies in the unpredictable value of i_pm during the dynamic process, which makes it impossible to predict the switching order and time between various modes. Therefore, the next step is mainly to verify the effectiveness of relay-switching strategy on oscillation frequency manipulation through numerical calculations. The operating conditions of each mode are as follows:

$$\begin{aligned}
\textbf{Mode } 1: &\begin{Bmatrix} i_\mathrm{p} \ge \alpha i_\mathrm{pm} \cap \\ \mathrm{d}i_\mathrm{p}/\mathrm{d}t \ge 0 \cap \\ i_\mathrm{s} \ge 0 \end{Bmatrix} \cup \begin{Bmatrix} i_\mathrm{p} \ge -\alpha i_\mathrm{pm} \cap \\ \mathrm{d}i_\mathrm{p}/\mathrm{d}t < 0 \cap \\ i_\mathrm{s} \ge 0 \end{Bmatrix} \\
\textbf{Mode } 2: &\begin{Bmatrix} i_\mathrm{p} \ge \alpha i_\mathrm{pm} \cap \\ \mathrm{d}i_\mathrm{p}/\mathrm{d}t \ge 0 \cap \\ i_\mathrm{s} < 0 \end{Bmatrix} \cup \begin{Bmatrix} i_\mathrm{p} \ge -\alpha i_\mathrm{pm} \cap \\ \mathrm{d}i_\mathrm{p}/\mathrm{d}t < 0 \cap \\ i_\mathrm{s} < 0 \end{Bmatrix} \\
\textbf{Mode } 3: &\begin{Bmatrix} i_\mathrm{p} < -\alpha i_\mathrm{pm} \cap \\ \mathrm{d}i_\mathrm{p}/\mathrm{d}t < 0 \cap \\ i_\mathrm{s} < 0 \end{Bmatrix} \cup \begin{Bmatrix} i_\mathrm{p} < \alpha i_\mathrm{pm} \cap \\ \mathrm{d}i_\mathrm{p}/\mathrm{d}t \ge 0 \cap \\ i_\mathrm{s} < 0 \end{Bmatrix} \\
\textbf{Mode } 4: &\begin{Bmatrix} i_\mathrm{p} < -\alpha i_\mathrm{pm} \cap \\ \mathrm{d}i_\mathrm{p}/\mathrm{d}t < 0 \cap \\ i_\mathrm{s} \ge 0 \end{Bmatrix} \cup \begin{Bmatrix} i_\mathrm{p} < \alpha i_\mathrm{pm} \cap \\ \mathrm{d}i_\mathrm{p}/\mathrm{d}t \ge 0 \cap \\ i_\mathrm{s} \ge 0 \end{Bmatrix}.
\end{aligned}$$

The autonomous system continuously switches between these four modes through the operating and switching conditions of the modes. Fig. 4 shows the dynamic response of the system at different thresholds, using the parameters listed in Table I. The ZPA frequency of autonomous oscillation in the simulation is slightly deviated from the calculation in the previous section due to the influence of higher harmonics [5]. The conservative switching strategy for the steady solution mentioned in the previous section allows the system to gradually transition from the single-modal to the multimodal region. However, it is found in the simulation that the system tends to operate in the low-frequency band when the initial value of α is greater than 0, and conversely the system tends to operate in the high-frequency band. Thus, the switching of the steady state solution does not have to be strictly from single-modal region to multimodal region. When α switches from 0 to -0.2, the oscillation frequency

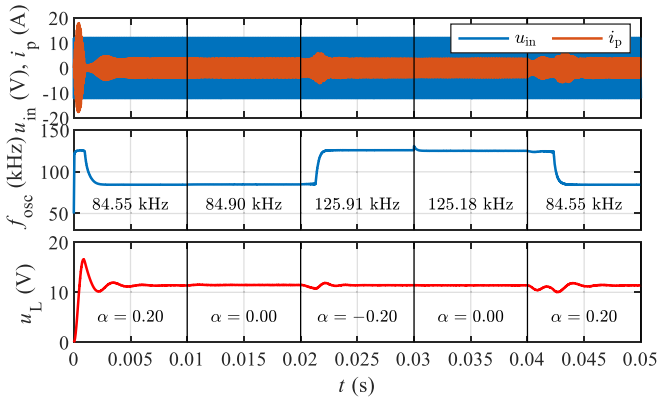

Fig. 4. Oscillation frequency manipulation by adjusting the threshold of relay. Top: Input voltage and current. Middle: Oscillation frequency. Bottom: Load voltage.

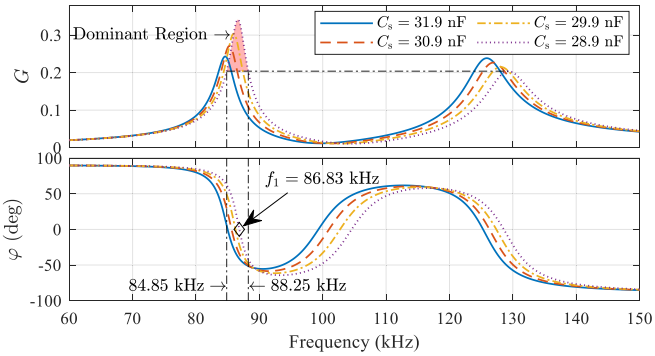

Fig. 5. Frequency responses by detuning the secondary resonator. Top: Input current to voltage amplitude ratio. Bottom: Phase difference between the input current and voltage.

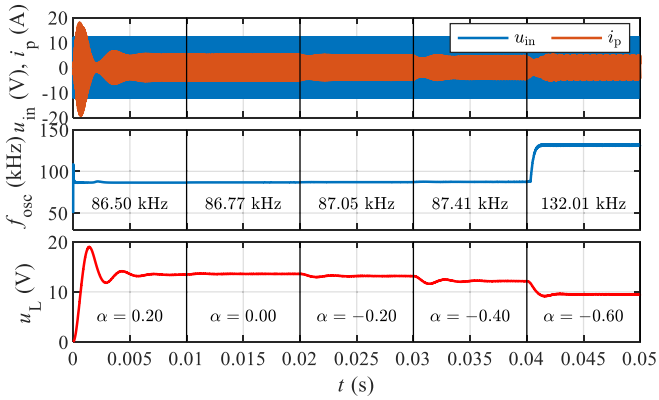

Fig. 6. Convergence to unique oscillation frequency insensitive to threshold variation by detuning the secondary resonator ($C_s = 28.9$ nF). Top: Input voltage and current. Middle: Oscillation frequency. Bottom: Load voltage.

jumps from 84.90 to 125.91 kHz. When α switches back from -0.2 to 0, the system is still in the high-frequency band. This shows there are at least two oscillation frequencies for the system when $\alpha = 0$, and also that the final oscillation frequency may be different under different initial conditions.

The phenomenon of oscillation frequency hopping can be roughly explained from the amplitude gain curve of the system. When $\varphi \in [\varphi_1, 0]$, as can be seen from the top part of Fig. 3, the amplitude gain in the high-frequency band $[f_2, f_{2H}]$ is generally larger than that in the low-frequency band $[f_1, f_{1H}]$, so the self-excitation mechanism tends to magnify the high-frequency components of i_p, which makes the oscillation frequency converge to the high-frequency band. On the contrary, when $\varphi \in [0, \varphi_2]$, the low-frequency components of i_p become dominant and the oscillation frequency converges to the low-frequency band $[f_{1L}, f_1]$.

It should be noted that the relay-switching strategy used to manipulate the oscillation frequency exhibits hysteresis, as evidenced in Fig. 4, where the change of α from –0.2 to 0 does not significantly affect the oscillation frequency. This indicates the existence of an attraction region where the oscillation frequency remains stable despite changes in α. This is a favorable feature as it enhances frequency stability against potential disturbances in α. In the next section, we show that the proposed gain shaping method can significantly expand this region of attraction.

B. Forcing Low Oscillation Frequency With Zero-Voltage Switch (ZVS)

In practical applications, it is necessary to make the system operate at a weakly inductive state to achieve ZVS. However, there exist two inductive regions and the oscillation frequency sometimes falls into the high-frequency band. In this case, the switching and ac losses of the system increase, and it may also violate the permitted range of operation. To address this issue, we propose a gain shaping method to reshape the gain curve to ensure a weakly inductive state of the system in the low-frequency range.

Gain shaping can be realized by detuning the primary or secondary resonator. In this letter, we tune the secondary compensation capacitor. Fig. 5 shows the frequency responses of the system under different C_s. Clearly, the gain in the low-frequency band is enlarged as C_s decreases, while the gain in the high-frequency band is attenuated at the same time. This makes the oscillation characteristics of the system mainly dominated by the low-frequency band, i.e., the shadowed area in Fig. 5, thereby increasing the probability of converging to the low-frequency band. The dynamic response of the system during threshold variation is shown in Fig. 6. The threshold range corresponding to the low-frequency band has been expanded to -0.4, which is sufficient to ensure that the system oscillation frequency is stable as well as to allow the system to operate simultaneously in a low-frequency and weakly inductive state to obtain ZVS conditions.

C. Discussion

Relay-switching strategy can enable the system to operate within the desired frequency band. However, due to the unpredictable nature of i_{pm} during dynamic processes, establishing a mathematical model to analyze the system's nonlinear dynamic behavior poses a challenge. Moreover, while gain is the primary

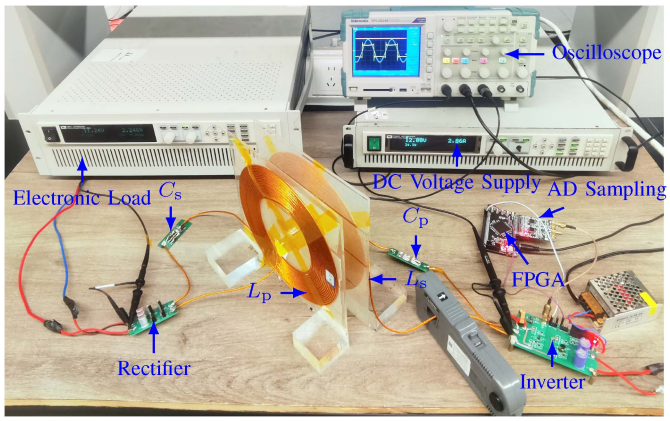

Fig. 7. Experimental setup.

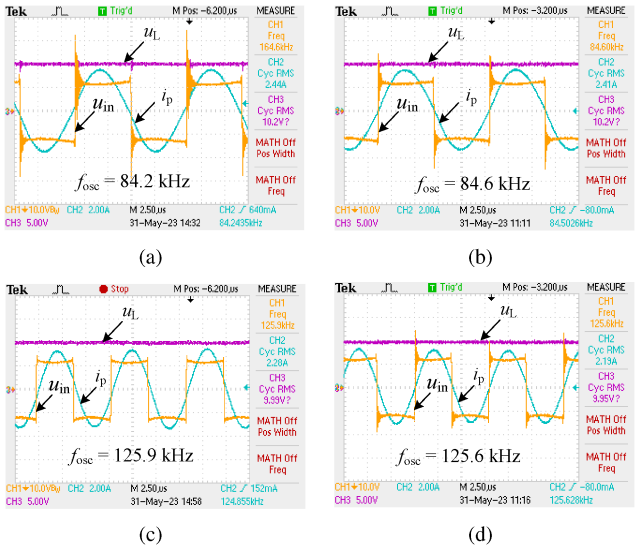

Fig. 8. Waveforms of inverter voltage, current, and output voltage under different thresholds ($C_s = 31.9$ nF). (a) $\alpha = 0.2$. (b) $\alpha = 0$. (c) $\alpha = -0.2$. (d) $\alpha = 0$.

factor influencing the convergence of the oscillation frequency, components, such as the rectifier and dc bus capacitance might also affect the system's stability. Future research will concentrate on developing mathematical models and investigating the influence of nonlinear elements on the stability of autonomous WPT systems.

IV. Experimental Verfication

Fig. 7 shows the experimental setup (the parameters are listed in Table I), where an analog to digital converter AD9226, with a sampling rate of 65 Msps, is used to sample the input current, while a field programmable gate array EP4CE10E22C8N is used as the controller. The coupler parameters are measured through the IM3536 LCR bridge. The high-frequency noise of current sampling is filtered out through a low-pass digital filter.

Fig. 8 shows the steady-state voltage and current waveforms of the system at different thresholds. The error between the oscillation frequency of the experiment and the simulation frequency

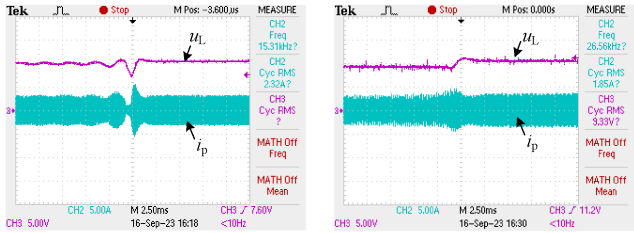

Fig. 9. Dynamic process of switching between oscillation frequencies. (a) Threshold α is switched from –0.05 to –0.1, and the oscillation frequency is switched from low-frequency to high-frequency band. (b) Threshold α is switched from 0.05 to 0.1, and the oscillation frequency is switched from high-frequency to low-frequency band.

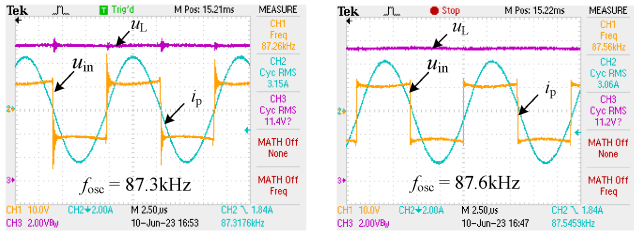

Fig. 10. System waveform after gain curve shaping with $C_s = 28.9$ nF. (a) $\alpha = 0$. (b) $\alpha = -0.2$.

is mainly caused by the error of the resonant capacitor and the losses of the switching devices. In Fig. 8(a), the system is in the capacitive region and in a hard switching state, with significant switching noise. In Fig. 8(b) and (c), the system is in a ZPA state. When α is switched from 0.2 to -0.2, the system crosses from the capacitive region to the inductive region. It is worth noting that when α is switched from 0 to -0.2, the system jumps from the low-frequency band to the high-frequency band. As shown in Fig. 9(a), a notable dynamic process of oscillation frequency switching is captured when α switched from -0.05 to -0.1. When α is switched from -0.2 to 0, the system is still in the high-frequency band. The notable dynamic process of the transition from the low-frequency band to the high-frequency band is shown in Fig. 9(b), with a switching operation for α from 0.05 to 0.1. The experiment confirms that the autonomous WPT system has multiple steady-state solutions in the multimodal region, and can be switched between different steady-state points by adjusting the threshold. Moreover, it seems that the transferred power and dc/dc efficiency at 84.6 kHz are, respectively, 20.8 W and 81.6%, and both outperform that at 125.6 kHz (19.2 W and 81.1%). Despite f_0 is unstable in an autonomous state, the system can be transitioned from a closed-loop to an open-loop to operate at f_0. An efficiency of 82.1% was noted at $f_0 = 99.3$ kHz under open-loop conditions.

Fig. 10 shows the results of the system after shaping the gain curve. The oscillation is in the low-frequency band irrespective to the variation of α, eliminating the phenomenon of frequency hopping and being designed within the standard range specified for WPT.

V. Conclusion

This letter proposes an autonomous WPT system with relay switch. By adjusting the threshold, free switching between multiple steady-state solutions can be achieved. Furthermore, by reshaping the gain curve of the input current, the system can operate in a low-frequency weakly inductive state. Future work will aim to provide more theoretical analysis and practical insights into the nonlinear dynamic behavior of the proposed system.

References

[1] A. Namadmalan, "Self-oscillating tuning loops for series resonant inductive power transfer systems," *IEEE Trans. Power Electron.*, vol. 31, no. 10, pp. 7320–7327, Oct. 2016.

[2] S. Assawaworrarit, X. Yu, and S. Fan, "Robust wireless power transfer using a nonlinear parity–time-symmetric circuit," *Nature*, vol. 546, no. 7658, pp. 387–390, Jun. 2017.

[3] S. Assawaworrarit and S. Fan, "Robust and efficient wireless power transfer using a switch-mode implementation of a nonlinear parity–time symmetric circuit," *Nature Electron.*, vol. 3, no. 5, pp. 273–279, May 2020.

[4] J. Zhou, B. Zhang, W. Xiao, D. Qiu, and Y. Chen, "Nonlinear parity-time-symmetric model for constant efficiency wireless power transfer: Application to a drone-in-flight wireless charging platform," *IEEE Trans. Ind. Electron.*, vol. 66, no. 5, pp. 4097–4107, May 2019.

[5] C. S. Tang, Y. Sun, Y. G. Su, S. K. Nguang, and A. P. Hu, "Determining multiple steady-state ZCS operating points of a switch-mode contactless power transfer system," *IEEE Trans. Power Electron.*, vol. 24, no. 2, pp. 416–425, Feb. 2009.

[6] Z. Hua, K. T. Chau, W. Liu, and X. Tian, "Pulse frequency modulation for parity-time-symmetric wireless power transfer system," *IEEE Trans. Magn.*, vol. 58, no. 8, Aug. 2022, Art. no. 8002005.

[7] Z. Hua, K. T. Chau, W. Liu, X. Tian, and H. Pang, "Autonomous pulse frequency modulation for wireless battery charging with zero-voltage switching," *IEEE Trans. Ind. Electron.*, vol. 70, no. 9, pp. 8959–8969, Sep. 2023.